# Segmented Block Copolymers with Monodisperse Hard Segments: The Influence of H-Bonding on Various Properties

Gerard J. E. Biemond,* Jan Feijen, Reinoud J. Gaymans*

The properties of segmented-copolymer-based H-bonding and non-H-bonding crystallisable segments and poly(tetramethylene oxide) segments were studied. The crystallisable segments were monodisperse in length and the non-hydrogen-bonding segments were made of tetraamidepiperazineterephthalamide (TPTPT). The polymers were characterised by DSC, FT-IR, SAXS and DMTA. The mechanical properties were studied by tensile, compression set and tensile set measurements. The TPTPT segmented copolymers displayed low glass transition temperatures (T_g, $-70\,°C$), good low-temperature properties, moderate moduli ($G' \approx 10–33$ MPa) and high melting temperatures (185–220 °C). However, as compared to H-bonded segments, both the modulus and the yield stress were relatively low.

1.0 µm
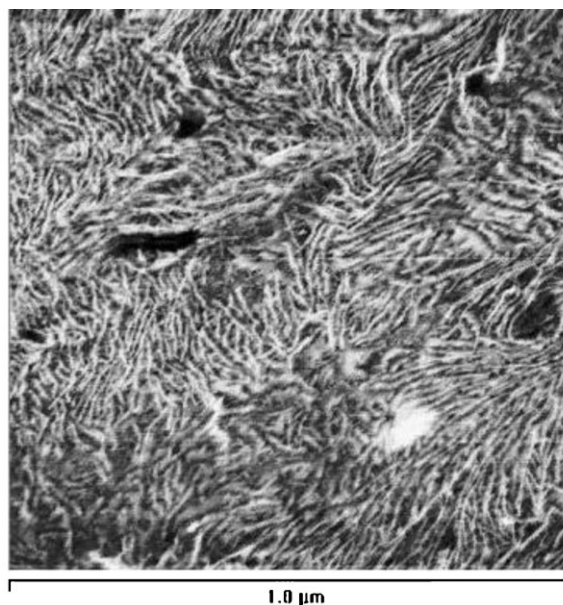
Introduction

Hydrogen bonding has a strong influence on the physical and chemical properties of polymers, such as the melting temperature, solubility and adhesion.[1] Hydrogen bonds are relatively strong secondary forces that increase the chain interaction in both the crystalline and amorphous states. However, hydrogen bonding is not a necessity for crystallisation. For example, polyethylene does not display hydrogen bonding or strong secondary forces but still crystallises easily and to a high degree.[2] This is a result of the polyethylene having a perfectly regular structure, being flexible and demonstrating a tight packing. Nevertheless, hydrogen-bonding plays an important role with regard to numerous polymer properties, and thus, most nylons have higher melting temperatures, yield and fracture stresses as compared to polyethylene.[3]

Non-H-bonding polyurethanes, comprised of poly(tetramethylene oxide) (PTMO) and *n*-alkyl urethanes with piperazine units, have been well described.[4–9] In these studies, the urethane segments were monodisperse in length and the repeat length of the alkyl unit was varied from 2 to 4. The polyurethanes containing piperazine exhibited an increased thermal stability as it did not show

G. J. E. Biemond, J. Feijen, R. J. Gaymans
Department of Science and Technology, University of Twente, P.O. Box 217, 7500 AE, Enschede, The Netherlands
E-mail: r.j.gaymans@utwente.nL;
g.j.e.biemond@alumnus.utwente.nL
G. J. E. Biemond
Polymer Institute, P.O. Box 902, 5600 AX Eindhoven, The Netherlands
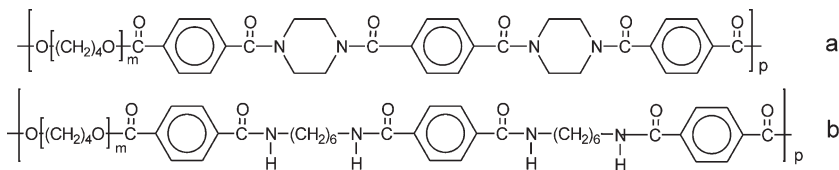Current address: SABIC Europe, Geleen, The Netherlands

Figure 1. Segmented block copolymers based on (a) non-hydrogen-bonding PTMO$_x$-TPTPT segments and (b) hydrogen-bonding crystallisable PTMO$_x$-T6T6T segments.

trans-urethanisation. As compared to hydrogen-bonded polyurethanes, the piperazine polyurethanes have a glass transition at low temperature ($-50\,^\circ$C), only slightly temperature-dependent rubber modulus, high fracture strains but also high tensile set (TS) values. Such non-H-bonding polyurethanes with monodisperse hard segments show very interesting properties.

Segmented block copolymers with monodisperse amide segments have also been investigated.[10–16] The amide segments in these copolymers consisted of primary amines and the amides were able to form H-bonds. A typical copolymer was comprised of PTMO and hexamethylene-diamineterephthalamide (T6T6T), a tetra-amide based on terephthalic acid (T) and hexamethylenediamine units (6) (Figure 1b).[12,13,15,16]

Segmented copolymers based on tetraamides have been found to crystallise fast and almost completely and forming crystalline ribbons with high aspect ratios.[12–16] The moduli of the copolymers increased considerably with increasing amide content and could be approximated using a model for fibre-reinforced polymers.[13,14] With mono-disperse segments, the modulus from room temperature to near melting of the polymer was almost independent of temperature and the melting transition was sharp.[6–16] Also the elastic properties, i.e., the compression set (CS), TS and stress relaxation, were good.[12–16] It is as of yet unclear to what extent these properties were due to the H-bonding.

As for the polyurethanes discussed above, non-hydrogen-bonding amides can be prepared using the secondary piperazine amine.[17] By choosing to utilize piperazine instead of ethylene diamine, the melting temperature was reduced by 100$\,^\circ$C and the amide chain mobility was found to occur at a lower temperature. The piperazine unit has a non-planar, alicyclic structure that can present either a chair or boat conformation.

The present paper discusses the synthesis and properties of segmented copolymers based on PTMO and tetraami-depiperazineterephthalamide (TPTPT) units of uniform length (Figure 1a). This TPTPT segment had tertiary amide groups and was therefore unable to form hydrogen bonds. The properties of the resulting PTMO$_x$-TPTPT copolymer without H-bonding were compared to those of segmented PTMO$_x$-T6T6T copolymers but with hydrogen bonding. Such a direct comparison between hydrogen-bonding and non-hydrogen-bonding amide systems provided insight

into the influence of H-bonding in segmented block copolymers on the properties.

Experimental Part

Materials

Dimethyl terephthalate, *N*-methyl-2-pyrrolidone (NMP), phenol, 1,2,4-trichlorobenzene and toluene were purchased from Aldrich and used as received. Tetraisopropyl orthotitanate [Ti(i-OC$_3$H$_7$)$_4$] was also purchased from Aldrich and was diluted in *m*-xylene (to 0.05 M), which was purchased from Merck. PTMO with a length of 1 000 and 2 000 g $\cdot$ mol^{-1} were generously donated by Dupont. Irganox 1330 was obtained from Cíba. The synthesis of methylphenyl terephthalate (MPT)[14], the PTMO$_x$-T6T6T copolymers[15] and diphenyl terephthalate (DPT) were carried out as described in ref.[14]

Synthesis of 1-[4-(piperazine-1-ylcarbonyl)benzoyl]piperazine

In a first step 1-[4-(piperazine-1-ylcarbonyl)benzoyl]piperazine was synthesised. Piperazine (120 g, 1.4 mol) was melted at 140 $^\circ$C in a round-bottomed flask with a nitrogen inlet, mechanical stirrer and a reflux condenser, and then reacted with DPT (39 g, 0.12 mol) for 16 h at 140 $^\circ$C. The product was a transparent liquid that partly solidified during the reaction. Two litres of methanol were added to the reaction mixture to dissolve the product and part of the methanol was subsequently distilled off until 0.5 l of the solution remained. Upon addition of ether (1 l) to the solution, a white product precipitated. This product, denoted PTP, was collected by filtration over a no. 4 glass filter. The yield of the reaction was 67%, and the product had a melting peak, as measured by DSC, of 198 $^\circ$C with a melting enthalpy of 70 J $\cdot$ g^{-1}. The purity of the product, estimated from NMR spectra, was found to be >95%.

^{1}H NMR (TFA-*d*): $\delta = 7.68$ (s, 4H, terephthalic H), 4.34 (s, 4H, CH$_2$ piperazine terephthalic side), 3.97 (s, 4H, CH$_2$ piperazine NH side), 3.71 (s, 4H, CH$_2$ piperazine terephthalic side), 3.55 (s, 4H, CH$_2$ piperazine NH side).

Synthesis of Tetraamidepiperazineterephthalamidedimethyl

In a second step, the PTP units were reacted with MPT to give TPTPT-dimethyl. In a round-bottomed flask, PTP-piperazine (85 g, 0.28 mol) was dissolved in trichlorobenzene at 120 $^\circ$C. To this solution, MPT (200 g, 0.8 mol) was added and the reaction was carried out at 140 $^\circ$C for 16 h under a nitrogen flow. After one hour, a white product started to precipitate from the solution. The product was collected by filtration of the hot solution over a heated no.4 glass filter and washed three times with acetone. TPTPT-dimethyl had a melting temperature of 250 $^\circ$C and a melting enthalpy of 40 J $\cdot$ g^{-1}, as determined by DSC. The purity estimated from NMR spectra was found to be >95%.

^{1}H NMR (TFA-d): $\delta = 8.28$ (t, 4H, terephthalic H ester side), 7.69 (s, 4H, terephthalic H, centre terephthalic), 7.6–7.75 (t, 4H, terephthalic H, piperazine side), 4.2 (d, 4H, CH$_2$ piperazine), 4.12 (d, 6H, methyl endgroup), 4.05 (s, 4H, CH$_2$ piperazine), 3.82 (s, 4H, CH$_2$ piperazine), 3.66 (d, 4H, CH$_2$ piperazine).

Poly(tetramethylene oxide)tetraamidepiperazineterephthalamide Polymerisation

The polymerisation was carried out in a 250 mL stainless steel reactor with a nitrogen inlet and a magnetic coupling stirrer. The polymerisation of PTMO$_{1\,000}$ with TPTPT-dimethyl is given as an example. The reactor was charged with PTMO$_{1\,000}$ (50 g, 0.05 mol), TPTPT-dimethyl (34.3 g, 0.05 mol), 100 mL NMP, 1 wt.-% Irganox 1330 (based on PTMO) and a catalyst solution [5 mL of 0.05 M Ti-(i-OC$_3$H$_7$)$_4$ in m-xylene] under a flow of nitrogen. The stirred reaction mixture was heated to 180 °C in 30 min, to 250 °C and then maintained at 250 °C for 2 h. Subsequently, the pressure was carefully reduced ($P < 20$ mbar) to distil off the NMP and then further reduced ($P < 0.3$ mbar) after which the mixture was allowed to react for 60 min. Finally the reactor was cooled slowly, with the low pressure maintained. The resulting copolymers were transparent and tough. ^{1}H NMR analysis in TFA-d gave the following peaks: $\delta = 8.36$ (t, 4H, terephthalic H, ester side), 7.69 (s, 4H, terephthalic H, centre terephthalic), 7.6–7.85 (t, 4H, terephthalic H, piperazine side), 4.6 (s, 4H, CH$_2$ PTMO, ester side), 4.28 (s, 4H, CH$_2$ piperazine), 4.13 (s, 4H, CH$_2$ piperazine), 3.88 (m, 52H, CH$_2$ PTMO), 3.74 (s, 4H, CH$_2$ piperazine), 2.07 (t, 8H, CH$_2$ PTMO, ester side), 1.91 (s, 48H, CH$_2$ PTMO, ether side).

^{1}H NMR

NMR spectra were recorded with a Bruker AC 300 spectrometer at 300 MHz. Deuterated trifluoroacetic acid (TFA-d) was used as the solvent.

Viscometry

The solution viscosities were measured at a concentration of 0.1 dl·g^{-1} in a mixture of phenol/1,1,2,2-tetrachloroethane (1:1 molar ratio) at 25 °C using a capillary Ubbelohde type 1B viscometer. The inherent viscosities were calculated.

Differential Scanning Calorimetry

DSC thermograms were recorded on a Perkin-Elmer DSC apparatus, equipped with a PE7700 computer and a TAS-7 software. Dried samples of 5–10 mg were heated to approximately 30 °C above their melting temperature, subsequently cooled and heated again. The heating and cooling rates were both 20 °C·min^{-1}. The crystallisation temperature (T_c) was taken as the temperature location of the maximum of the crystallisation peak in the first cooling scan. The temperature location of the maximum of the melting peak in the second heating scan was taken as the melting

temperature and also the melting enthalpy could be determined from this peak. The degree of crystallinity was calculated from the melting enthalpy of the polymer and the melting enthalpy of the bisester tetraamide according to:

$$X_c(\text{DSC}) = \frac{\Delta H_{\text{m polymer}}}{\Delta H_{\text{m bisester tetraamide}} \times \text{Conc}_{\text{tetraamide}}} \qquad (1)$$

Fourier-Transform Infrared (FT-IR) Spectroscopy

Infrared transmission spectra were recorded using a Nicolet 20SXB FT-IR spectrometer with a resolution of 4 cm^{-1}. The samples to be measured were prepared by adding a drop of the polymer dissolved in HFIP (1 g·l^{-1}) onto a pressed KBr pellet. Temperature-dependent FT-IR spectra were recorded between 25 and 210 °C.

Atomic Force Microscopy (AFM)

AFM measurements were recorded on a Nanoscope IV controller (Veeco) operating in tapping mode. The AFM was equipped with a J-scanner with a maximum size of 200 μm^2. Si-cantilevers (Veeco) were used to obtain height and phase images. The amplitude in free oscillation was 5.0 V. The operating set-point value (A/A_0) was set to relatively low values of 0.70, the size of the scans was 1×1 μm^2. Solvent-cast samples with thicknesses of ≈ 20 μm were prepared on a silicon wafer from a 3 wt.-% solution in trifluoroacetic acid (TFA).

Synchrotron SAXS

Small angle X-ray scattering (SAXS) experiments were performed on the Dutch-Belgium (DUBBLE) beamline BM26 at the European Synchrotron Radiation Facility (ESRF) in Grenoble, France. The wavelength of the beam was 1.2 Å. A two-dimensional SAXS detector was used and the range for the scattering vector (q) was 0–1.8 nm^{-1}. Temperature-dependent profiles were recorded with a Linkam remote-controlled DSC stage at a heating and cooling rate of 10 °C·min^{-1}. The background was subtracted from the intensity. The two dimensional SAXS intensity was azimuthally integrated to obtain the scattering pattern as a function of $q = 2 \sin \theta/\lambda$ and the long spacing (L, in nm) was calculated from $L = 2\pi \cdot q^{-1}$.

Dynamic Mechanical Thermal Analysis (DMTA)

Samples ($70 \times 9 \times 2$ mm^3) for DMTA were prepared using an Arburg H manual injection moulding machine with a barrel temperature that was set 50 °C above the melting temperature of the copolymer. The mould was kept at room temperature. The test samples were dried *in vacuo* at 50 °C for 24 h before use. DMTA thermograms were recorded on a Myrenne ATM3 torsion pendulum at a frequency of 1 Hz and 0.1% strain. The storage (G') and loss (G'') moduli were measured as functions of temperature. The samples were cooled to -100 °C and subsequently heated at a rate of 1 °C·min^{-1}. The temperature location of the maximum of the loss modulus peak was taken as the glass transition temperature. The start of the

rubber plateau was denoted the flex temperature (T_{flex}), and the flow temperature (T_{flow}) was defined as the temperature where the storage modulus reached 1 MPa. The stability of the rubber plateau can be described according to the following expression:

$$\Delta G' = \frac{G'_{(T_{flex})} - G'_{(T_{flow}-50\,°C)}}{G'_{25\,°C}} \times \frac{1}{\Delta T}(°C^{-1}) \qquad (2)$$

Here, ΔT represents the temperature range: $\Delta T = (T_{flow} - 50\,°C) - T_{flex}$.

Tensile Testing

Stress/strain curves were obtained on injection-moulded, 2.2 mm thick dumbbells (ISO37 type 2), using a Zwick Z020 universal tensile machine equipped with a 500 N load cell. The strain was measured with extensometers. The tensile tests were carried out at an initial strain rate of $0.4\,s^{-1}$ (test speed of $60\,mm \cdot min^{-1}$). For test temperatures other than room temperature, a temperature-controlled environment chamber was used. The E-moduli at each temperature were determined in eight-fold at strains from 0.1–0.25%. The standard deviation of the modulus was 5–8%. Also measured were the yield stress (σ_y), the yield strain (ε_y), the fracture stress (σ_b), the fracture strain (ε_b) and the true fracture stress (σ_{true}). The true fracture stress was obtained by multiplying σ_b by the straining factor $[=1+(\varepsilon_b/100)]$. For each test three samples were used and the average taken.

Compression Set

Samples for CS experiments were cut from injection moulded bars and investigated at room temperature according to the ASTM 395 B standard. A compression was applied and maintained for 24 h at room temperature before being released. After a relaxation period of half an hour, the thickness of the samples was measured. The CS, defined according to Equation (3), was taken as the average of three measurements.

$$\text{Compression set} = \frac{d_0 - d_2}{d_0 - d_1} \times 100\% \qquad (3)$$

In the above expression, d_0 is the thickness before compression (mm), d_1 is the compressed thickness (mm) and d_2 is the thickness 30 min after releasing the compression (mm).

Tensile Set

Cyclic stress/strain experiments were conducted on the injection-moulded bars cut into dumbbells (ISO 37 type 2). A Zwick Z020 universal tensile machine equipped with a 500 N load cell was used to measure the stress as a function of the strain of each loading and unloading cycle at a strain rate of $60\,mm \cdot min^{-1}$. The strain of each loading-unloading cycle was increased (stair-case loading) and the TS of the strain increment was determined as a function of the applied strain. The incremental TS was calculated from the

following relation:

$$\text{Tensile set} = \frac{\Delta \varepsilon_{remaining}}{\Delta \varepsilon_{cycle}} = \frac{\varepsilon_{r,cycle(i)} - \varepsilon_{r,cycle(i-1)}}{\Delta \varepsilon_{cycle}} \times 100\% \qquad (4)$$

where $\varepsilon_{r,\,cycle(i)}$ is the remaining strain at the end of cycle i and $\varepsilon_{r,\,cycle(i-1)}$ is the remaining strain at the end of the preceding cycle $i-1$. Directly after the stress was zero, a new cycle was started and for each following cycle, the strain was increased by 20%.

Results and Discussion

Segmented copolymers based on PTMO and monodisperse tetraamidediester units were synthesised (Figure 1). The TPTPT was unable to form hydrogen bonds, while T6T6T was capable of H-bonding. The starting material for the tetraamidediester was either a TPTPT-dimethyl (T_m 250 °C, ΔH_m 40 $J \cdot g^{-1}$) or a hexamethylenediamineterephthalamide (T6T6T-dimethyl) (T_m 303, ΔH_m 150 $J \cdot g^{-1}$).[18] The TPTPT-dimethyl unit compared to T6T6T-dimethyl had a lower melting temperature and a lower heat of fusion. This was a result of two opposing effects, the flexible hexamethylene group being replaced by the cyclic piperazine group and the H-bonding in T6T6T was absent in TPTPT. The low heat of fusion was believed to be due to difficulties in obtaining close-packing caused by the non-planar piperazine group and mixtures of the chain-boat conformations. The segmented copolymers were made up of PTMO with an $\overline{M}_n$ of either 1 000 or 2 000 $g \cdot mol^{-1}$ and denoted $PTMO_{1\,000}$ and $PTMO_{2\,000}$.

PTMO$_x$, TPTPT, T6T6T Segmented Copolymers

The PTMO$_x$-tetra-amide segmented copolymers were prepared in a solution/melt polymerization process. The synthesised copolymers were transparent in the melt and thus melt phasing did not occur. Upon cooling, the polymers were found to be tough, elastic and transparent materials with high inherent viscosities (Table 1).

FT-IR Spectroscopy

The FT-IR spectrum of $PTMO_{1\,000}$-TPTPT was very similar to that of TPTPT-dimethyl, apart from the 1 100 cm^{-1} band of the PTMO (Figure 2).

The copolymers displayed the carbonyl bands of esters and amides in the wave length region of 1 600–1 750 cm^{-1}. For $PTMO_{1\,000}$-TPTPT, two peaks could be seen: one at 1 630 cm^{-1} assigned to the amide carbonyl next to the piperazine ring and a second peak at 1 730 cm^{-1} attributed to the ester carbonyl group. These peak positions were similar to those of the TPTPT-dimethyl starting material.

Table 1. Thermal properties from DSC analysis of the copolymers based on $PTMO_{1000}$ and $PTMO_{2000}$.

Sample	Tetraamide	η_{inh}	T_m	T_c	$T_m - T_c$	ΔH_m	ΔH_c	X_c (DSC)
	%	$dL \cdot g^{-1}$	°C	°C	°C	$J \cdot g^{-1}$	$J \cdot g^{-1}$	%
$PTMO_{1000}$-TPTPT	32.5	1.95	226	203	23	10	9	77
$PTMO_{2000}$-TPTPT	19.8	1.5	–	–	–	–	–	–
$PTMO_{1000}$-T6T6T	35.0	2.0	241	229	12	43	36	82
$PTMO_{2000}$-T6T6T	21.6	2.2	229	218	11	32	20	86

The amide carbonyl peak was stronger than that of the ester carbonyl as the ratio of amide to ester was 4:2. Since piperazine is a tertiary amide without a proton at the amide, the (N–H) amide bands at $3\,300$ and $1\,540\,cm^{-1}$ were not observed. Upon increasing the temperature of $PTMO_{1000}$-TPTPT, only small changes in the spectrum were observed and it could be concluded that neither the ester nor amide carbonyl in this copolymer was sensitive to crystalline order.

$PTMO_{1000}$-T6T6T displayed a crystalline amide carbonyl peak at $1\,625\,cm^{-1}$, an amorphous amide carbonyl peak at $1\,670\,cm^{-1}$ and an ester carbonyl peak at $1\,720\,cm^{-1}$.[14] Upon heating the $PTMO_{1000}$-T6T6T material, the crystalline amide peak at $1\,625\,cm^{-1}$ decreased in size while the size of the amorphous amide carbonyl peak at $1\,670\,cm^{-1}$ increased. From this change, the T6T6T crystallinity could be determined and was found to be very high (92%).[14] In the FT-IR, the band for the ether group (C–O–C stretching) at PTMO $1\,110\,cm^{-1}$ and for the methylene groups of hexamethylene diamine and the polyether were at $1\,437$, $1\,283$ and $1\,254\,cm^{-1}$.

DSC

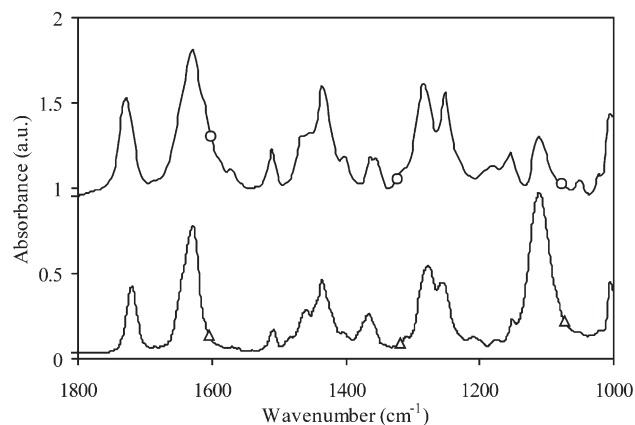Also the melting and crystallisation behaviour of the $PTMO_x$-tetra-amide copolymers were studied by DSC. For $PTMO_{2000}$-TPTPT, no melting or crystallisation transition could be observed. The heating and cooling thermograms for $PTMO_{1000}$-TPTPT and $PTMO_{1000}$-T6T6T can be seen in Figure 3.

The cooling curves of both copolymers displayed a small peak next to the main crystallisation peak. A second transition was also observed in the second heating scan of $PTMO_{1000}$-TPTPT. Such additional transitions – often observed with polyamides – are thought to be due to a solid state transition (Brill temperatures).[12–15] The melting and crystallisation temperature for $PTMO_{1000}$-TPTPT was approximately 15 °C lower than for $PTMO_{1000}$-T6T6T (Table 1), and the $T_m - T_c$ values were very low for both systems. The $PTMO_{1000}$-TPTPT copolymer demonstrated low melting and crystallisation enthalpies of about $10\,J \cdot g^{-1}$.

The melting enthalpy of the TPTPT-dimethyl unit was $40\,J \cdot g^{-1}$ and this value was used to calculate the crystallinity of the TPTPT segment in the copolymer according to Equation (1). The obtained crystallinity was found to be high despite the crystalline packing that might not be all that neat. The crystallinities of $PTMO_{1000}$-T6T6T and $PTMO_{2000}$-T6T6T were calculated in a similar fashion and were also found to be high. Moreover, these crystallinities

Figure 2. FT-IR spectra of the TPTPT-dimethyl unit (○) and the polymer $PTMO_{1000}$-TPTPT (△).
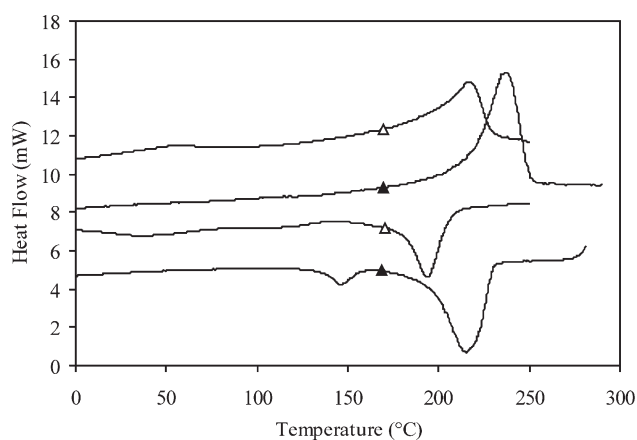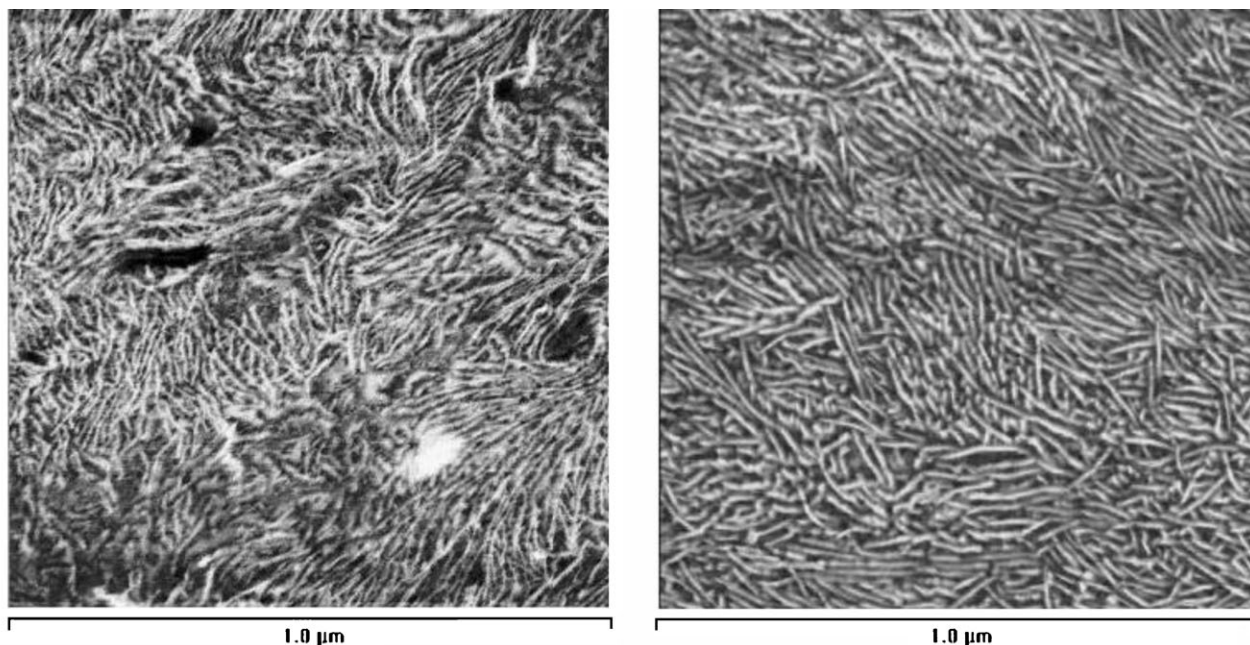

Figure 3. DSC heating and cooling traces of segmented copolymers without hydrogen bonding segments (TPTPT) and with hydrogen bonding segments (T6T6T); △: $PTMO_{1000}$-TPTPT, ▲: $PTMO_{1000}$-T6T6T.

■ *Figure 4.* AFM micrographs of $PTMO_{2\,000}$-TPTPT (left) and $PTMO_{2\,000}$-T6T6T(right).

corresponded well with the crystallinities as determined by FT-IR. Thus, the TPTPT units in the copolymer displayed lower melting temperatures and lower values of heat of fusion than their T6T6T counterparts. Nonetheless, the crystallinity of the TPTPT segment in the copolymer remained high.

AFM

The morphology of the $PTMO_{2\,000}$-TPTPT and $PTMO_{2\,000}$-T6T6T copolymers was studied by AFM on cast films. In phase angle mode, white ribbons were observed and these corresponded to the TPTPT and T6T6T crystallites (Figure 4). The lengths of the ribbons were determined to be several hundreds of nanometres. The extended length of the TPTPT and T6T6T units were 2.8 and 3.6 nm, respectively, with a chain direction of the units perpendicular to the ribbon length. It is clear from Figure 4 that the TPTPT ribbons were shorter than their crystalline T6T6T counterparts, and the aspect ratio of the TPTPT ribbons was thus expected to be lower than for T6T6T.

SAXS

The average repeat distance of crystalline segments, the so-called long spacing, can be obtained from SAXS measurements. As was demonstrated above, the copolymers displayed crystallites with a ribbon-like structure. These ribbons had three dimensions: the ribbon length, thickness and width. The ribbon length was a few hundred nanometres and the ribbon thickness, i.e., the extended

length of the tetra-amide, was approximately 2.8–3.6 nm. The third dimension, the width of the ribbons, is known to vary with the crystallization conditions. At room temperature, the $PTMO_{1\,000}$-TPTPT copolymer had a long spacing of 12.0 nm and $PTMO_{1\,000}$-T6T6T had one of 15.3 nm. This suggests that the width of the T6T6T ribbons (i.e., the third direction) was somewhat wider in these samples which indicate that the crystallisation in the width direction occur faster for T6T6T than for TPTPT.

Upon heating of semi-crystalline polymers, a gradual melting of the crystallites takes place and the long spacing increased steadily with temperature.[14] The long spacing of both $PTMO_{1\,000}$-TPTPT and $PTMO_{1\,000}$-T6T6T was studied as a function of temperature in a thermal cycle to temperatures above the melting temperature of the materials (Figure 5). The long spacing of $PTMO_{1\,000}$-TPTPT was found to be constant up to near-melting temperatures and $PTMO_{1\,000}$-T6T6T demonstrated a similar behaviour.

Upon cooling, the long spacing decreased and this was more gradual than on melting. The fully crystalline state was obtained after some time. This hysteresis in the long spacing was stronger for the TPTPT segments than for the T6T6T segments, indicating that the T6T6T segments crystallised faster.

DMTA

The shear storage and loss moduli of the $PTMO_x$-TPTPT copolymers as functions of temperature are presented in Figure 6 and the DMTA data of all the copolymers is presented in Table 2.
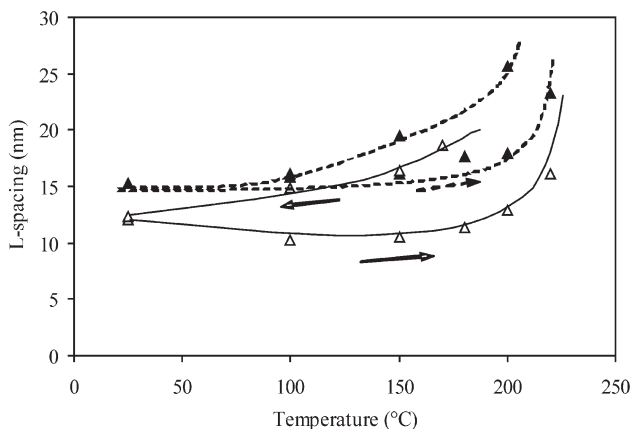
Figure 5. The *L*-spacing as a function of temperature for hydro-gen-bonded and non-hydrogen-bonded segmented copolymers: △, PTMO$_{1000}$-TPTPT; ▲, PTMO$_{1000}$-T6T6T.
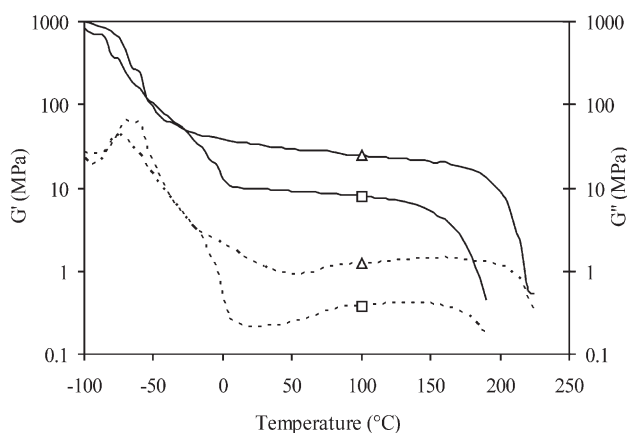

Figure 6. The storage (solid line, left axis) and loss (dotted line, right axis) moduli as functions of temperature for segmented block copolymers based on PTMO and uniform TPTPT segments; △: PTMO$_{1000}$-TPTPT, □: PTMO$_{2000}$-TPTPT.

Two transitions could be observed, a glass transition near −70 °C and melting around 200 °C. The glass transition temperatures were extremely low, suggesting a very small content of TPTPT in the PTMO phase. The glass transition temperatures for TPTPT seemed to be even lower than for T6T6T. This difference was also observed in the piperazine-based polyurethanes. For PTMO$_{2000}$, a shoulder on the peak

representing the glass transition was observed at −10 °C and was believed to be caused by the melting of the PTMO$_{2000}$. It is known that PTMO segments with lengths above 1 400 g · mol^{-1} are capable of crystallising.[12–16,19] The start of the rubbery plateau (T_{flex}) was very low for PTMO$_{1000}$, and was not influenced by the crystallisation of PTMO. The rubber modulus in the plateau region was only little temperature dependent and the melting transition was sharp. Such behaviour is typical for copolymers with crystallisable segments of uniform length.

However, the modulus of the TPTPT copolymers at room temperature, was three times lower than the modulus of their T6T6T counterparts (Table 2). Possible explanations for these lower moduli include a lower crystallinity, a lower aspect ratio of the crystallites and/or less stiff TPTPT crystallites. The crystallinity of the TPTPT segments was determined by DSC not to be lower; however, the heat of fusion value was considerably lower (Table 1). This difference in heat of fusion suggests a less dense packing of the crystallites. The AFM analysis indicated that the TPTPT crystallites had a smaller aspect ratio (Figure 4).

The flow temperatures of the copolymers, obtained by DMTA, corresponded very well with the melting temperatures as measured by DSC (Table 1). The melting temperature of the TPTPT segmented copolymers were, as compared to the T6T6T copolymers, influenced by two opposing factors: the absence of hydrogen bonding and the increased stiffness of the piperazine units as compared to the hexamethylene units. The melting temperature of TPTPT was thus 15–35 °C lower.

Tensile Properties

The stress/strain curves of the segmented block copolymers with and without hydrogen bonding are shown in Figure 7. No necking was observed during the tensile measurement.

The *E*-modulus for TPTPT segmented polymers was much lower than for their T6T6T counterparts (Table 3). Moreover, the yield stress was a factor of two lower for the TPTPT copolymers than for the T6T6T materials. Thus, the stress necessary to deform the non-hydrogen-bonding TPTPT crystallites was lower than for the H-bonded T6T6T. The underlying reason was the absence of hydrogen bonding

Table 2. DMTA properties of PTMO$_x$-TPTPT and PTMO$_x$-T6T6T.

Sample	Hard segment	η_{inh}	T_g	T_{flex}	G′ $_{25\,°C}$	$\Delta G'$	T_{flow}	CS	TS$_{50\%}$
	%	dL · g^{-1}	°C	°C	MPa	10^3 K^{-1}	°C	%	%
PTMO$_{1000}$-TPTPT	32.5	1.95	−67	−35	33	4.7	220	28	29
PTMO$_{2000}$-TPTPT	19.8	1.5	−75	5	9.8	3.5	185	22	13
PTMO$_{1000}$-T6T6T	35.0	2.0	−61	−15	87	3.7	240	18	33
PTMO$_{2000}$-T6T6T	21.6	2.2	−68	5	39	1.7	225	13	17
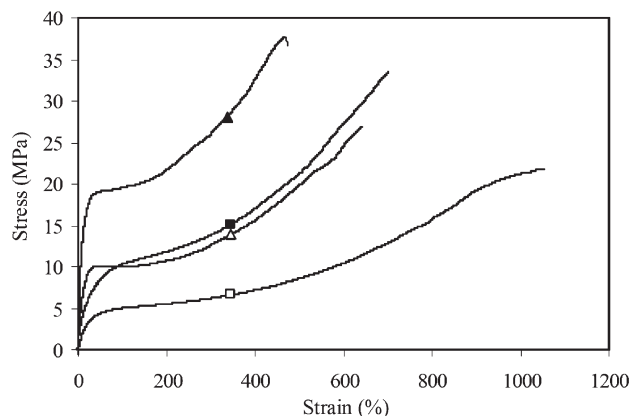
Figure 7. Stress/strain curve; △: PTMO$_{1\,000}$-TPTPT, □: PTMO$_{2\,000}$-TPTPT, ▲: PTMO$_{1\,000}$-T6T6T, ■: PTMO$_{2\,000}$-T6T6T.

Figure 8. The CS, performed at 25% compression at room temperature, as a function of modulus; □: PTMO$_x$-TPTPT, ■: PTMO$_x$-T6T6T.

and the poorer crystalline packing. The yield strain, on the other hand, was found to be approximately the same for the non-hydrogen-bonding segmented copolymers as for those with H-bonds.

After the yield point, strain hardening of the PTMO phase occurred, thus increasing the strength of both copolymers. The fracture stresses of the TPTPT polymers were lower than for their T6T6T counterparts, however, the fracture strains were higher. The fracture stress and strain can be combined into a single parameter known as the true fracture stress σ_{true}. Surprisingly, the values of true fracture stress increased with the PTMO length (i.e., with a decreasing amide content) (Table 3). Moreover, the true fracture stresses were similar for the TPTPT and the T6T6T copolymers. This suggests that the fracture properties were more dependent on the polyether phase than on the content or aspect ratio of the crystallized amide segments. The higher true fracture stresses for the PTMO$_{2\,000}$ compared to PTMO$_{1\,000}$ must have been due to strain hardening occurring more readily for this segment.

Compression Set

A standard means of investigating the elastic behaviour of segmented copolymers is by CS experiments. The CS values
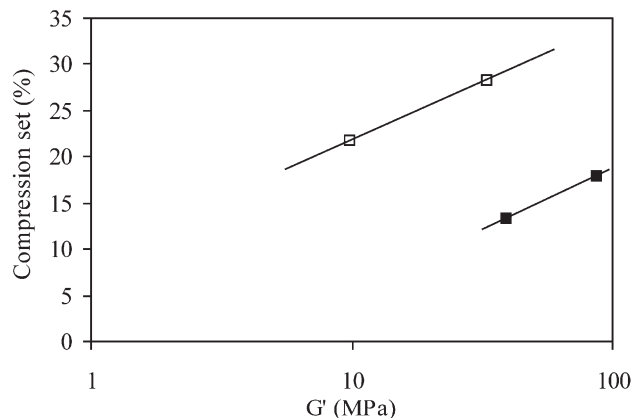
of the copolymers in the present study were found to increase with decreasing PTMO length (Table 2). The CS values were somewhat higher for PTMO$_x$-TPTPT as opposed to for PTMO$_x$-T6T6T, and these higher CS values must have been due to more easily deformable crystallites caused by the absence of hydrogen bonding as well as by the inferior packing of TPTPT in the crystalline state. A general trend in copolymers is that the CS values increase with increasing modulus and both the PTMO$_x$-TPTPT and PTMO$_x$-T6T6T copolymers complied with this behaviour (Figure 8). However, the CS-values in the G''/CS graph for the TPTPT copolymers were particularly high as the TPTPT copolymers displayed both lower moduli and higher CS values.

Tensile Set

Another way to study the elastic properties of polymers is by TS experiments; the TS as a function of strain is particularly informative. In these experiments, the strain of each loading-unloading cycle was increased (stair-case loading) and the TS of the strain increment was determined as a function of the applied strain. All of the PTMO$_x$-TPTPT and PTMO$_x$-T6T6T copolymers were studied and the results are presented in Figure 9. The TS curves for TPTPT showed

Table 3. The tensile properties of PTMO$_x$-TPTPT and PTMO$_x$-T6T6T.

Sample	Hard segment	η_{inh}	E-modulus	σ_y	ε_y	σ_b	ε_b	σ_{true} [1]
	%	dL·g^{-1}	MPa	MPa	%	MPa	%	MPa
PTMO$_{1\,000}$-TPTPT	32.5	1.95	140	10	27	28	642	208
PTMO$_{2\,000}$-TPTPT	19.8	1.9	33	4	48	22	1 050	253
PTMO$_{1\,000}$-T6T6T	35.0	2.0	333	18	25	38	468	216
PTMO$_{2\,000}$-T6T6T	21.6	2.2	110	9	57	33	702	265

[1] $\sigma_{\text{true}} = \lambda \cdot \sigma_{\text{break}}$.
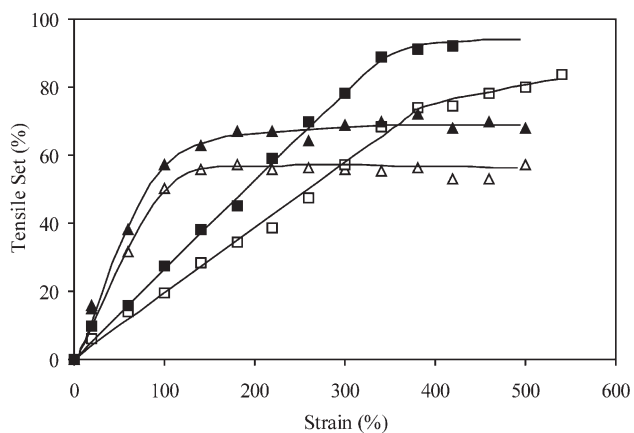
Figure 9. The TS as a function of strain; △: PTMO$_{1\,000}$-TPTPT, □: PTMO$_{2\,000}$-TPTPT, ▲: PTMO$_{1\,000}$-T6T6T, ■: PTMO$_{2\,000}$-T6T6T.

the same trend as those for T6T6T. With PTMO$_{1\,000}$, the TS values increased up to a strain of about 100% and then flattened out. The curves for the TPTPT materials displayed lower TS values than their T6T6T counterparts. With PTMO$_{2\,000}$, the TS increased up to a strain of about 350% before reaching a plateau. The reason why the TS values were ultimately higher for the PTMO$_{2\,000}$ segments as opposed to PTMO$_{1\,000}$ was the strain crystallisation of the former. Also in this case the TPTPT materials display lower values than their T6T6T counterparts. The TPTPT copolymers were thus more elastic, however at a lower modulus of the material (Table 2).

The TS at 50% strain (TS$_{50\%}$) is a typical value. With increasing modulus, TS$_{50\%}$ values are generally known to increase.[12–14] For PTMO$_x$-T6T6T, the TS$_{50\%}$ was in accordance with the results from the PTMO$_x$-T6A6T series,[14] and the TS$_{50\%}$ as a function of the modulus displayed higher values for the PTMO$_x$-TPTPT materials that were thus found to be less elastic at a particular stiffness (Figure 10).
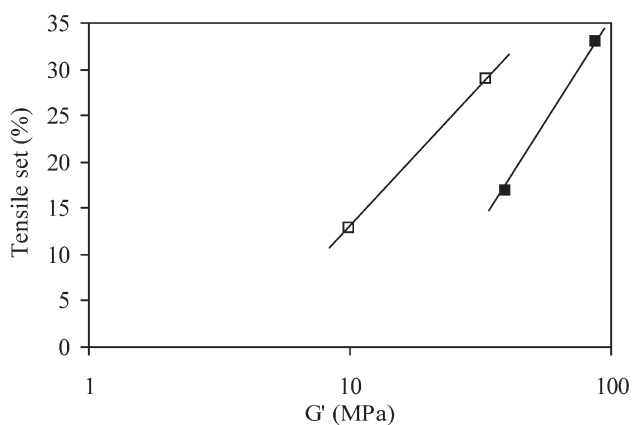

Figure 10. TS$_{50\%}$ as a function of the modulus at 25 °C; □: PTMO$_x$-TPTPT, ■: PTMO$_x$-T6T6T.

Conclusion

Segmented PTMO$_x$-TPTPT copolymers with non-hydrogen-bonding monodisperse crystallisable TPTPT segments were studied. The polymerisation was carried out with a TPTPT-dimethyl unit that was synthesised prior to the poly-condensation reaction to ensure the uniformity of the segment. This TPTPT-dimethyl unit had a particularly low heat of melting, suggesting a not so tight crystalline packing. This inferior close-packing might be due to the non-planar structure and a mixture of chain/boat con-formations of the piperazine unit. The PTMO$_x$-TPTPT copolymers could be melt-processed and the molecular weight of the samples was high. The PTMO$_x$-TPTPT copolymers displayed a melting temperature of about 200 °C as well as a low melting enthalpy. Despite this low melting enthalpy, the crystallinity of the TPTPT segments in the copolymer was high. The TPTPT segments in the copolymers formed nanoribbons but the aspect ratio of these ribbons did not seem to be very high. The SAXS pattern indicated a well-crystallised morphology.

The PTMO$_x$-TPTPT segmented copolymers displayed a low glass transition temperature (−70 °C), suggesting an almost complete crystallisation of the monodisperse amide segments. The copolymers had a temperature-independent rubber modulus in the rubber region, as often observed with monodisperse crystallisable segments, but the moduli of the copolymers were lower than those of the PTMO$_x$-T6T6T copolymers. Also the yield stresses were low for the materials with TPTPT segments. The change in yield stress followed the change in the modulus, and these low modulus and yield stress values for the PTMO$_x$-TPTPT copolymers were thought to be a result of the lower reinforcing effect of the crystallites arising from the absence of hydrogen bonding, a poorer crystalline packing and the lower aspect ratio of the crystallites.

The fracture stresses for the TPTPT copolymers were lower than for the T6T6T copolymer; however, the true fracture stresses were equivalent. However, these true fracture stresses were dominated by the polyether seg-ments. The elastic properties, as measured by CS and TS, as functions of the stiffness were poorer for the TPTPT copolymers as opposed to for the T6T6T materials. This was due to the lower aspect ratio of the crystallites and their poorer packing, probably as a result of the non-planar structure and chair/boat conformations of the piperazine units.

DOI: 10.1002/mame.200900093

[1] B. Kaczmarczyk, D. Sek, *Polymer* **1995**, *36*, 5019.
[2] A. J. Peacock, *Handbook of Polyethylene: Structures, Properties, and Applications*, Marcel Dekker, New York 2000.
[3] M. I. Kohan, *Nylon Plastics Handbook*, Hanser, Munich 1995.
[4] L. L. Harrel, *Macromolecules* **1969**, *2*, 607.
[5] H. N. Ng, *Polymer* **1973**, *14*, 255.
[6] A. E. Allegrezza, R. W. Seymour, H. N. Ng, S. L. Cooper, *Polymer* **1974**, *15*, 433.
[7] C. D. Eisenbach, H. Nefzger, in: *Multiphase Macromolecular Systems, Contemporary Topics in Polymer Science*, Vol. 6, W. M. Cumbertson, Ed., Plenum, New York 1989, p. 339.
[8] N. Reynolds, H. W. Spiess, H. Hayen, H. Nefzger, C. D. Eisenbach, *Macromol. Chem. Phys.* **1994**, *195*, 2855.
[9] C. D. Eisenbach, T. Heinemann, *Macromolecules* **1995**, *28*, 2133.
[10] R. J. Gaymans, J. L. de Haan, *Polymer* **1993**, *34*, 4360.
[11] M. C. J. E. Niesten, J. Feijen, R. J. Gaymans, *Polymer* **2000**, *41*, 8487.
[12] J. Krijgsman, D. Husken, R. J. Gaymans, *Polymer* **2003**, *44*, 7573.
[13] M. J. van der Schuur, R. J. Gaymans, *J. Polym. Sci., Part A. : Polym. Chem. Ed.* **2006**, *44*, 4769.
[14] G. J. E. Biemond, J. Feijen, R. J. Gaymans, *J. Appl. Polym. Sci.* **2007**, *105*, 951.
[15] G. J. E. Biemond, Dissertation, University of Twente, The Netherlands 2006, Ch 6.
[16] D. Husken, J. Feijen, R. J. Gaymans, *J. Polym. Sci., Part A: Polym. Chem. Ed.* **2007**, *45*, 4522.
[17] B. Vanhaecht, J. de Vroede, W. Rudolph, M. Biesemans, G. Wyjayanthi, S. Rastogi, S. Hoffmann, P. G. Klein, C. E. Koning, *J. Polym. Sci., Part A. : Polym. Chem. Ed.* **2003**, *41*, 2082.
[18] J. Krijgsman, D. Husken, R. J. Gaymans, *Polymer* **2003**, *44*, 7043.
[19] P. Dreyfuss, M. P. Dreyfuss, G. Pruckmayr, in: *Encyclopedia of Polymer Science and Engineering*, Vol. 16, H. Mark, N. Bikales, C. Overberger, G. Menges, Eds., *Wiley*, New York 1989, p. 649.